HHS Public Access

Author manuscript

Prog Neurobiol. Author manuscript; available in PMC 2021 November 06.

Published in final edited form as:

Prog Neurobiol. 2021 May ; 200: 101985. doi:10.1016/j.pneurobio.2020.101985.

Altered striatum centered brain structures in *SHANK3* deficient Chinese children with genotype and phenotype profiling

Chunxue Liu[a,1], **Dongyun Li**[a,1], **Haowei Yang**[b], **Huiping Li**[a], **Qiong Xu**[a], **Bingrui Zhou**[a], **Chunchun Hu**[a], **Chunyang Li**[a], **Yi Wang**[a], **Zhongwei Qiao**[b,*], **Yong-hui Jiang**[c,*], **Xiu Xu**[a,*]

[a]Department of Child Health Care, Children's Hospital of Fudan University, 399 Wanyuan Road, Shanghai, China

[b]Department of Radiology, Children's Hospital of Fudan University, 399 Wanyuan Road, Shanghai, China

[c]Department of Genetics, Pediatrics and Neuroscience, Yale University School of Medicine, New Heaven CT 06520 USA

Abstract

SHANK3 deficiency represents one of the most replicated monogenic risk factors for autism spectrum disorder (ASD) and *SHANK3* caused ASD presents a unique opportunity to understand the underlying neuropathological mechanisms of ASD. In this study, genetic tests, comprehensive clinical and neurobehavioral evaluations, as well as multimodal structural MRI using voxel-based morphometry (VBM) and tract-based spatial statistics (TBSS) were conducted in SHANK3 group (N = 14 with *SHANK3* defects), ASD controls (N = 26 with idiopathic ASD without *SHANK3* defects) and typically developing (TD) controls (N = 32). Phenotypically, we reported several new features in Chinese *SHANK3* deficient children including anteverted nares, sensory stimulation seeking, dental abnormalities and hematological problems. In SHANK3 group, VBM revealed decreased grey matter volumes mainly in dorsal striatum, amygdala, hippocampus and parahippocampal gyrus; TBSS demonstrated decreased fractional anisotropy in multiple tracts involving projection, association and commissural fibers, including middle cerebral peduncle, corpus callosum, superior longitudinal fasciculus, corona radiata, external and internal capsule, and posterior thalamic radiation, etc. We report that the disrupted striatum centered brain structures are associated with *SHANK3* deficient children. Study of subjects with monogenic cause offer specific insights into the neuroimaging studies of ASD. The discovery may support a path for future functional connectivity studies to allow for more in-depth understandings of the abnormal neural circuits and the underlying neuropathological mechanisms for ASD.

*Corresponding authors. qiaozhwei@163.com (Z. Qiao), yong-hui.jiang@yale.edu (Y.-h. Jiang), xuxiu@shmu.edu.cn (X. Xu).
[1]Contribute equally.

Declaration of Competing Interest

None.

Appendix A. Supplementary data

Supplementary material related to this article can be found, in the online version, at doi:https://doi.org/10.1016/j.pneurobio.2020.101985.

Keywords

SHANK3; Autism spectrum disorder; Brain imaging; Voxel-based morphometry; Tract-based spatial statistics; Striatum

1. Introduction

Despite the substantial progress of genomics discoveries, the underlying neuropathophysiology of autism spectrum disorder (ASD) remains largely uncharacterized in humans. Brain imaging via different modalities have been used extensively to delineate the structural and functional connectivity in human ASD (D'Albis et al., 2018; Hernandez et al., 2015; Muller and Fishman, 2018). A long list of neuroimaging studies in literature discovered differences in a numerous brain regions or tracts between ASD and controls (Aoki et al., 2017; Ecker et al., 2015; Muhle et al., 2018; Swanson et al., 2018; Varghese et al., 2017; Wolff et al., 2017). Several prospective studies have supported the predictive value of early imaging findings of cortical surface and brain volume including cortico-striatal, thalamo-striatal, hippocampus and limbic system for the diagnosis of ASD (Bostan et al., 2013; Li et al., 2017; Utter and Basso, 2008). However, the majority of the results and conclusions are inconsistent. The etiological and clinical heterogeneity may be the major reasons contributing to the variability of findings. The lack of understanding for the etiology of studying subjects also makes it difficult to probe these findings at mechanistic level.
To address these caveats in the experimental designs and data interpretation, one of the strategies is to conduct the study in a homogenous subgroup of ASD with confirmed genetic etiology. This has only become feasible recently because of genomic discovery of reproducible mutations in single gene in a significant sub-set of ASD (Durand et al., 2007; Jordan et al., 2019; Willsey and State, 2015). However, few brain imaging studies have been conducted prospectively with appropriate controls and integrate the clinical and behavioral features in genetic caused ASD so far (Mahmood et al., 2010; Maillard et al., 2015; Tabet et al., 2017).

SHANK3 (SH3 and multiple ankyrin repeat domains 3) associated ASD present a unique opportunity to conduct this line of study because of recurrent genetic mutations and its immediate link to the synaptic physiology. SHANK3 is a master synaptic scaffolding protein enriched at the postsynaptic density of excitatory synapses that is crucial for synaptogenesis (Jiang and Ehlers, 2013; Monteiro and Feng, 2017; Sheng and Hoogenraad, 2007). Haploinsufficiency of *SHANK3* gene is a key contributor of autistic features in the 22q13.3 deletion syndrome (Phelan–McDermid Syndrome, PMS) (Bonaglia et al., 2011; Phelan and McDermid, 2012a; Phelan, 2008). Genomic sequencing studies have identified point mutations in *SHANK3* gene in idiopathic ASD and support the etiologic role of *SHANK3* in ASD (Betancur and Buxbaum, 2013; Bonaglia et al., 2011; Oberman et al., 2015a; Sarasua et al., 2014a, 2011). The majority of clinical features reported in subjects with *SHANK3* point mutations overlap with that the 22q13.3 deletion. Nevertheless, the speech impairment and motor deficit are more prominent in the individuals with 22q13 deletions than those with *SHANK3* point mutations (De Rubeis et al., 2018; Soorya et al., 2013). Currently, approximately 1% of ASD can be attributed to the genetic defects of

SHANK3 (Delahaye et al., 2009; Durand et al., 2007; Wilson et al., 2008) which makes *SHANK3* as one of most common and replicated genes from recent ASD genomics studies.

Modeling *SHANK3* deficiency in other organisms including *Drosophila*, zebrafish, mouse, rat, and non-human primate have provided evidence supporting a general role of *SHANK3* in synaptic development and function, and more specially, suggesting an important role of corticostriatal circuit in autism-like behaviors in these models (Chana et al., 2015; Liu et al., 2018; Pagani et al., 2019; Peca et al., 2011; Peixoto et al., 2016; Tu et al., 2019; Wang et al., 2016, 2011; Zhao et al., 2017; Zhou et al., 2019). However, the translational value of these findings to human *SHANK3* related ASD remains unclear due to the evolutional difference in brain structure and behavioral manifestations between human and other species (Chana et al., 2015; Peixoto et al., 2016; Wang et al., 2016).

In this study, we employed brain imaging study using voxel-based morphometry (VBM) and tract-based spatial statistics (TBSS) to investigate the grey matter and white matter alterations in cohorts of *SHANK3* deficient subjects, the idiopathic ASD, and typically developing children as controls respectively. Compared to traditional region-of-interest based analytic method, VBM is automated full-brain analysis without manually delineations; while TBSS provides advantages with higher spatial comparability. We attempted to assess the correlation of *SHANK3* genotype, clinical phenotype and brain structure with proper controls.

2. Materials and methods

2.1. Subjects

A total of 510 children diagnosed with ASD were consecutively recruited for genetic studies between August 1st, 2015 and August 31st, 2017 from the Division of Child Health Care, Children's Hospital of Fudan University. Blood samples were collected at first visit or revisiting to our outpatient clinic and Multiplex Ligation-dependent Probe Amplification (MLPA) technique was used to detect the deletion or duplication of *SHANK3* gene. Neuroimaging studies were conducted from March 1st, 2016 to September 31st, 2018. A total of 80 children in three groups (SHANK3 group, idiopathic ASD control, and typically developing control) were scanned and 8 subjects were excluded for the analysis due to the poor quality of images. Children with recognizable lesions or abnormalities on scans, cerebral palsy, or other neurologic or degenerative diseases were excluded. SHANK3 group: 14 participants were enrolled with *SHANK3* deletion or mutation. 2/14 with *SHANK3* deletion were screened out from 510 ASD children, 10/14 individuals were previously detected with *SHANK3* deletion by the genome-wide array Comparative Genomic Hybridization and confirmed *SHANK3* copy number variation by MLPA. The rest 2/14 were *SHANK3* mutations which were found by the Whole Exon Sequencing and confirmed by Sanger sequencing. Idiopathic ASD control group: 26 ASD children without *SHANK3* deficiency or known genetic etiology were recruited. Typically developing (TD) control group: 32 children underwent MRI scan because of first episode of febrile convulsion and paroxysmal dizziness or headache but otherwise normal developing children were used as normal controls.

This study was approved by ethics committee of Children's Hospital of Fudan University and all of the procedures were in accordance with the Declaration of Helsinki.

2.2. Clinical evaluations

1. Relevant medical records such as ultrasound of urinary system, echocardiogram and EEG were reviewed and documented.
2. Dysmorphological and neurological examinations were performed by clinical geneticist and pediatric neurologist during the clinical visit.
3. ASD diagnosis was based on the DSM-5 (Grzadzinski et al., 2013), ADOS-2 (Gotham et al., 2007) and Autism Diagnostic Interview-Revised (Lord et al., 1994) administrated by certified clinicians.
4. Griffiths Mental Development Scales (Griffiths) (Benatti et al., 1986) were conducted by licensed and certified clinicians to assess developmental and cognitive level which is applicable to the children with mental age (not physical age) from 0 to 8.

2.3. Genetic studies of SHANK3

MLPA of *SHANK3* was performed using a commercial *SHANK3*-special Probemix P339 MLPA kit (MRC-Holland, Amsterdam, Netherlands), which contains 37 probes in the *SHANK3* gene and 4 probes in 22q13.33. The assay was performed according to the manufacturer's protocols. Raw data were imported into GeneMarker software (SoftGenetics, State College, PA, USA) for MLPA analysis. After population normalization, data were compared with a synthetic control sample, which represents the median of all normal samples in the experiment. A threshold of dosage change <0.75 was used to identify deletions, and a threshold >1.30 was used to identify duplications.

SHANK3 point mutations were verified by Sanger sequencing. PCR was designed to amplify the target fragments from 15 ng genomic DNA of each family member. A 575-bp exonic fragment covering exon 21 (forward primer 5′- ggaagtcacccgaggacaag −3′, reverse primer 5′- gatggtgcttgtggtctcca −3′) was amplified. The amplified DNA fragments were then purified and sequenced on an ABI 3130 DNA analyzer using the BigDye Terminator v3.1 Cycle Sequencing kit (Applied Biosystems). Genomic locations are based on GRCh37 (hg 19).

2.4. MRI data acquisition

All MRI scans were obtained on a GE 3.0 T Discovery MR750 system (GE Medical Systems, Milwaukee, WI) with a 32-channel head coil at the Radiology Department after parental consent. Participants were routinely sedated in the "Sedation Center" under the supervision of a licensed clinician or anesthesiologist. Children are given chloral hydrate at a dose of 50 mg/kg orally approximately one hour prior to the MRI scan. Vital signs were monitored and recorded during the scan. High-resolution 3D T1-weighted BRAVO (BRA in Volume imaging) sequence was performed and the diffusion tensor imaging (DTI) data were acquired using spin-echo, echo planar sequence covering the entire brain. T1-weighted sequence parameters: repetition time (TR) =8.2 ms; echo time (TE) =3.2 ms; flip angle =

12°; voxel size = 1 × 1×1 mm^3; gap = 0; FOV = 256 mm; matrix = 256 × 256). DTI sequence parameters: 15 diffusion directions; b = 1000s/mm^2; repetition time (TR) =4600 ms; echo time (TE) =87.4 ms; flip angel = 90°; voxel size = 2*2*4 mm^3; gap = 0; FOV = 240 mm; matrix = 128 × 128; 15 b-factors 0 and 1000s/mm^2.

2.5. Voxel-based morphometry (VBM) analysis

VBM analysis was conducted with a fast diffeomorphic registration algorithm (Diffeomorphic Anatomical Registration using Exponentiated Lie algebra, DARTEL) (Ashburner, 2007) and CAT12 (http://dbm.neuro.uni-jena.de/cat/) toolboxes implemented in the Statistical Parametric Mapping software package (SPM12; http://www.fil.ion.ucl.ac.uk/spm/software/spm12/) on the platform of Matlab(Version R2014b, Mathworks Inc., USA). First, every structural scan was visually inspected, and images containing obvious artefacts were excluded. Besides, image quality rating (IQR) generated by CAT12 served as the parameter for imaging quality control (Table 1). Study-specific tissue probability maps were created using the Template-O-matic toolbox (Wilke et al., 2008). These tissue probability maps were subsequently applied in the DARTEL algorithm to produce the final templates for normalization and segmentation. Grey matter segmented images were submitted to the Check Sample Homogeneity by using the function embedded in CAT-12. Finally, the segmented images were smoothed with an 8 mm full-width at half maximum Gaussian kernel. At the end of this pre-processing, modulated, smoothed, normalized images were obtained for statistical analysis.

2.6. Tract-based spatial statistics (TBSS) analysis

DTI data were preprocessed and analyzed using the FSL software (Smith et al., 2004). First, structural patterns and artifacts for each subject were visually inspected. The 6 translational (x, y, z) and rotational (α, β, λ) head motion parameters were generated by SPM for each direction. The framewise displacement (FD) was then calculated based on the following formula:

$$\frac{1}{M-1}\sum_{i=2}^{M}\sqrt{|x_i-x_{i-1}|^2+|y_i-y_{i-1}|^2+|z_i-z_{i-1}|^2+|\alpha_i-\alpha_{i-1}|^2+|\beta_i-\beta_{i-1}|^2+|\gamma_i-\gamma_{i-1}|^2}$$

which is a modified version from Liu et al (Liu et al., 2008), where M is the number of directions (M = 15) in this study (Table 1). TBSS registrations to standard space were inspected for accuracy to make sure all data were properly aligned. The main preprocessing procedures included corrections for eddy current-induced artifacts and head motions, removing non-brain tissues, estimating the diffusion tensor and calculating the fractional anisotropy (FA) map and mean diffusivity (MD) map. Then, TBSS was applied to assess group level differences in the FA and MD maps (Smith et al., 2007). First, study-specific image registration procedures were applied. Every FA data were aligned to every other one to identify the “most representative” one as target for nonlinear registration. This target image was then affine-aligned into MNI152 standard space. Every FA map was transformed into MNI152 space by combining the nonlinear transform to the target FA image with the affine transform from that target to MNI152 space. Then the mean FA images and

mean FA skeletons were created. Statistical analyses were conducted based on projecting all subject's FA and MD values, respectively, onto the mean FA skeleton and submission of the 4D-projected FA and MD data.

2.7. Statistical analysis

Demographic and clinical data were analyzed using the statistical package SPSS 20.0. The threshold for all statistical significance was set at $p < 0.05$. Age, sex, total intracranial volume (TIV), total development quotient (DQ) from Griffiths scale, IQR for grey matter and FD for white matter were included as covariates.

For VBM, non-parametric permutation tests were performed using SnPM13 toolbox embedded in SPM12 (http://nisox.org/Software/SnPM13/). Age, sex, TIV, IQR and total DQ were included as covariates. One-way ANOVA was conducted among three groups and significant clusters were further picked up. Post-hoc t-tests between each two groups were performed taking the significant result of ANOVA as the explicit mask. The labelings are according to the Automated Anatomical Labeling (AAL) atlas (Tzourio-Mazoyer et al., 2002). Significance was set at $p < 0.05$ (FDR corrected).

For TBSS, group differences of both FA and MD values were analyzed with non-parametric permutation test and the statistical maps were processed at the cluster-level with Threshold-Free Cluster Enhancement. Age, sex, TIV, FD and total DQ were included as covariates. One-way ANOVA was conducted among three groups and significant clusters were further picked up. Post-hoc t-tests between each two groups were performed taking the significant result of ANOVA as the explicit mask. The labelings are according to the Johns Hopkins University (JHU) atlas (Wakana et al., 2004). The significance level was set at $p < 0.05$ (FWE corrected).

To further investigate the correlation between the brain structures and the clinical characteristics (deletion size, ADOS scale and Griffiths scale), we defined regions of interest (ROIs) based on the significant grey and white matter results between SHANK3 group and ASD controls (regions with voxel size <50 were excluded). Then we extracted the specific grey matter volumes of each subject for the above ROIs using SPM12 and MRIcron (www.mricro.com/mricron). FA and/or MD values of each subject were extracted basing on the FA and/or MD ROIs separately applying "cluster" and "fslmaths" tools embedded in FSL. The effects of age, TIV, DQ, FD for white matter and IQR for grey matter were firstly regressed for each ROI, and the residuals of the regression were used for the subsequent steps of correlation analysis. Spearman rank correlation for SHANK3 group and Pearson correlation for ASD group. Two-tailed $P < 0.05$ was set for statistical significance.

3. Results

3.1. Summary of the studying subjects

A total of 80 children in three groups were recruited for MRI scanning, of which the imaging data from 8 subjects were excluded after quality control. SHANK3 group: 14 participants (P1–14) were enrolled with *SHANK3* deletion or mutation (ages: 1.9–12.9 years, mean ± SD: 5.1 ± 3.1years, males: 6, females: 8). P8 and P10 were excluded in

the neuroimaging analysis due to the severe epilepsy (P8) and lack of ASD features (P10). Idiopathic ASD control group: 26 ASD children without *SHANK3* deficiency or known genetic etiology were recruited (ages: 1.8–10.6 years, mean ± SD: 4.0 ± 1.9 years, males: 22, females: 4). Typically developing (TD) control group: 32 children (ages: 1.8–9.8 years, mean ± SD: 5.0 ± 2.2 years, males: 22, females: 10) underwent MRI scan because of first episode of febrile convulsion and paroxysmal dizziness or headache but otherwise normal developing children were used as normal controls.

3.2. Molecular genetics of studying subjects

Among 14 patients in SHANK3 group, two patients with *SHANK3* gene deletion were identified from screening 510 (2/510) patients by MLPA with the positive rate of 0.4 %. Other 12 patients were recruited from the clinic that *SHANK3* defects were found in clinical genetic tests. Among 14 patients (Supplementary Table 1), 11/14 (P1–P11) had terminal deletions of 22q13.3 (Fig. 1A) with the deletion sizes ranging from 0.1–7.5 Mb (mean ± SD: 2.8 ± 2.3 Mb). P1–P10 exhibited deletions of entire *SHANK3* gene while P11 and P12 showed a small partial deletion of exons 9–22 and exons 4–8. P4, P8 and P11 had additional copy number variants of unknown significance in other chromosomes. P13 and P14 had indels of c.3984 del C (p.P1328fs) and c.4045_4046 del AC (p.T1349Tfs) respectively that resulted in the frameshift of the SHANK3 protein (Fig. 1B). Parental tests were performed for all subjects except P5 and P10 and indicated a *de novo* nature of these genetic mutations.

3.3. Clinical profiles of SHANK3 deficient subjects

3.3.1. Dysmorphology—A total of 29 dysmorphic features were evaluated and all patients had at least 9 abnormal features (Fig. 1C–E and Supplementary Table 2). The most common dysmorphic features were midface hypoplasia, wide nasal bridge, anteverted nares, poorly formed and large ears, long eyelashes and full cheeks present in 100 % of patients, followed by hypoplastic and dysplastic nails, large fleshy hands, and bulbous nose (>70 %). Notably, we have also found a few new and highly penetrant features including the anteverted nares (100 %) and dental dysplasia or hypoplasia (43 %), which extend the phenotypic spectrum for *SHANK3* associated disorders.

3.3.2. General growth and development—Growth patterns were mostly within the normal range. However, the short stature (<3th percentile, P8), underweight (<3th percentile, P3, P4 and P8) and microcephaly (<3SD, P4) had also been noted. Neonatal hypotonia was the first presenting symptom for all subjects which could contribute to poor feeding and feeble crying after birth (50 %). Hypotonia persisted through infancy and early childhood, as well as motor developmental delay (93 %), unsteady or abnormal gait (86 %), slobber/salivation (86 %), weak chewing (79 %), and a drowsy appearance (36 %).

Global developmental delay was prominent (Fig. 2A). Patients performed the best in the domain of gross motor and the worst in the domain of listening and language (<1st percentile). Ten patients (71 %) presented absent speech with no ability to even consciously call mom and dad (0 words, P1–P9 and P14).

3.3.3. Behavioral problems and medical comorbidities—Behavioral manifestations were assessed through parental interview (Supplementary Table 2). The most commonly reported symptoms were episodes of inattention (100 %), lack of risk perception (93 %), aggression (e.g. biting or beating, hair pulling, protruding tongue, bruxism, 79 %), and sensory stimulus seeking (64 %). Additionally, comorbidities including frequent respiratory infections (57 %), food and drug allergies (43 %), paraesthesia (36 %), seizures and constipation (29 %) were also present. Interestingly, hematological conditions including idiopathic thrombocytopenic purpura or anemia (21 %) was common which has not been reported previously.

3.3.4. Autism specific features—All of the patients have been evaluated with standardized assessments for ASD, including the DSM-5 and ADOS-2 or ADI-R scale (Supplementary Table 3). Thirteen out of fourteen patients (except P10, 93 %) met the criteria of DSM-5 for the ASD diagnosis. Results from the ADOS-2 indicated that 12/14 individuals met criteria for ASD (except P6 and P10). Weighted severity scores were also calculated to provide an estimate of ASD severity. The mean weighted severity score for patients with the diagnosis of ASD in our participants was 6.8 (SD 1.5). The ADI-R samples included 8 out of 14 participants since 6 patients were too young (<4 years) to administer. Strict interpretation of the ADI-R indicated that 6 out of 8 individuals (75 %, except P6 and P8) met full criteria on the ADI-R. An additional two participants (P6 and P8) met criteria in two out of three domains. The comprehensive diagnosis of ASD reached to 86 % (12/14), based on both standardized assessments (ADOS-2 or ADI-R) and DSM-5 criteria (Supplementary Table 3).

3.3.5. Comparison to non-SHANK3 ASD—Compared to idiopathic ASD patients, SHANK3 group exhibited a similar total score and severity in each domain of ADOS-2 but worse Griffiths scores in all of the developmental domains (Gross motor: $P<0.0001$; Social: $P = 0.002$; Language: $P<0.0001$; Fine motor: $P = 0.0004$; Adaptability: $P = 0.006$) (Fig. 2B–C and Table 1).

3.4. Altered structures of both grey and white matters for SHANK3 deficient subjects

No group differences were found in all of imaging quality controls parameters, including the 6 absolute head motion parameters, FD and IQR. Generally, TIV in children with S*HANK3* deficient was significantly less than those in ASD or TD group. Similarly, total FA values in the SHANK3 group were much less than that in other two groups while total MD values were just the reverse (Table 1).

VBM analysis and group comparisons were conducted between SHANK3 group (n = 12), ASD controls (n = 24) and TD controls (n = 25). We found that the grey matter volumes of the SHANK3 group was significantly less than those of the TD controls in four clusters which survived the FDR correction at $p < 0.05$. The peak MNI regions and coordinates (AAL) of the four clusters are right hippocampus (28.5, −6, −22.5), left amygdala (−27, 1.5, −19.5), right caudate (9, 10.5, −6) and left caudate (−7.5, 21, 0) respectively. The key regions involved were the bilateral hippocampus, amygdala, parahippocampus, putamen, olfactory and superior temporal pole (Fig. 3A and Supplementary Table 4). The comparison

between SHANK3 group and ASD controls showed significantly decreased grey matter volumes (P < 0.05, FDR corrected) in five clusters with peak MNI regions (AAL) in right hippocampus (27, −6, −22.5), left amygdala (−30, −4.5, −22.5), right caudate (9, 10.5, −6), left caudate (−9, 21, −3) and right middle occipital gyrus (28.5, −84, 4.5). The mainly involved regions included bilateral hippocampus, amygdala, putamen and caudate and right parahippocampus olfactory, pallidum and middle occipital gyrus (Fig.3A and C, Table 2). However, no increased grey matter volumes in SHANK3 group than ASD controls and no significant differences for VBM results between ASD group and TD group were found.

The general white matter morphometry analysis in the whole brain showed that SHANK3 group exhibited significant reduction in FA value and increase in MD value than TD and ASD controls (Table 1). To further inquire into the statistical outcomes, we then conducted TBSS analysis for FA and MD across participants for each point of the common skeleton. Compared with TD controls, SHANK3 group showed markedly decreased FA in multiple regions ($P < 0.05$, FWE corrected). The most significant reductions of FA were found in the middle cerebellar peduncle, corpus callosum, corona radiata, superior longitudinal fasciculus, external capsule, posterior thalamic radiation, internal capsule, cingulum, and etc. (cluster 1, $P = 0.002$; cluster 2, $P = 0.004$) (Fig. 3B and Supplementary Table 5). However, no regions showed increased FA in SHANK3 group than TD controls and no significant difference for MD between two groups were found.

To compare with ASD, SHANK3 group showed decreased FA in middle cerebellar peduncle, corpus callosum, corona radiata, superior longitudinal fasciculus, external capsule, posterior thalamic radiation, internal capsule, cingulum, cerebral peduncle, sagittal stratum, tapetum and uncinated fasciculus (cluster 1, $P = 0.002$; cluster 2, $P = 0.004$) (Fig. 3B–C and Table 3). However, no tract with increased FA in SHANK3 group than ASD controls were found and no significant MD differences between two groups were found.

3.5. Correlation analyses between brain imaging findings and clinical characteristics

We further examined whether there is any correlation between structural changes in brain and clinical characteristics in either SHANK3 group or ASD group with age, sex, TIV, total DQ, IQR or FD were included as covariates.

For grey matter (Fig.4 A–B and Supplementary Table 6), ROIs were defined by the overlap between the VBM results and the AAL template including left amygdala ROI, right parahippocampus ROI, right putamen ROI, caudate ROI and hippocampus ROI. Positive correlation found in the SHANK3 group was left amygdala ROI volume and the RRB score of ADOS (r = 0.579, $P = 0.048$). For white matter (Fig.4D–H and Supplementary Table 6), FA values were extracted for specific tracts based on the overlap between the TBSS results (Table 3) and the ICBM-DTI-81 white-matter labels atlas. Positive correlations were found in the SHANK3 group between FA values of overall TBSS results and DQ of Griffith domains including social domain (r = 0.621, $P = 0.041$), language domain (r=0.744, $P = 0.009$), fine motor domain (r=0.781, $P = 0.005$) and performance domain (r=0.729, $P = 0.011$). Correlations between FA values on specific tracts and the clinical characteristics were not significant.

In addition, hippocampus ROI volume was positively associated with the RRB score of ADOS (r = 0.467, $P = 0.029$) in the ASD group but not in the SHANK3 group. The correlation between the deletion size and the neuroimaging metrics were insignificant in SHANK3 group (Supplementary Table 6).

4. Discussion

In the present work, we report a cohort of *SHANK3* deficient Chinese children with comprehensive clinical, neurobehavioral, and brain imaging assessments. Structural brain MRI revealed decreased total intracranial volume, grey matter volumes in striatum centered regions including dorsal striatum, amygdala, hippocampus and parahippocampal gyrus as well as decreased FA values in multiple white matter tracts involving projection, association and commissural fibers, including middle cerebellar peduncle, corpus callosum, corona radiata, superior longitudinal fasciculus, external capsule, internal capsule, posterior thalamic radiation and etc. Furthermore, the significant correlations between these regional grey/white matter alterations and the levels of different developmental domains or severity of ASD core symptoms help to explain why *SHANK3* patients mainly demonstrate developmental delay and autistic features. Worth to mention, in contrast with previous brain imaging studies for ASD (Ecker et al., 2015; Li et al., 2017; Mahmood et al., 2010; Maillard et al., 2015; Muhle et al., 2018; Tabet et al., 2017), the subjects of the present study carry homogenous highly penetrant genetic cause with a reasonable sample size of the controls (both idiopathic ASD and typically developing children as controls).

Most of children in present study have terminal deletions of 22q13.3 with the deletion sizes ranging from 0.1 to 7.5 Mb (mean ± SD: 2.8 ± 2.3 Mb) (Fig.1A). *SHANK3* is one of more than 50 genes within the largest 7.5 Mb deletion. It is clear that *SHANK3* gene, mapping to the distal end of 22q13.33, is disrupted in all cases in our study and the deficiency of SHANK3 is considered to contribute to the key neurologic characteristics seen in patients with terminal 22q13.3 deletion (Lek et al., 2016; Phelan and McDermid, 2012a; Sarasua et al., 2014b). It is noted other genes are also variably deleted in 22q13.3 deletion syndrome patients. The haploinsufficiency of other genes could also modify the effect of *SHANK3* mutation and may contribute to the neurobehavioral and MRI phenotypes in these subjects (Sarasua et al., 2014a; Soorya et al., 2013). Further genotype and phenotype correlation studies among subjects with variable size of deletions are warranted to understand the contribution of other genes in the region.

The clinical features in *SHANK3*-deficient patients in our study are largely consistent with the findings in other reports of children with *SHANK3* deficient from different populations (Oberman et al., 2015b; Phelan and McDermid, 2012b; Philippe et al., 2008a; Xu et al., 2020; Zwanenburg et al., 2016). Global developmental delay (especially speech delay), ASD, hypotonia were the most common features in different races. However, we noted a few unique facial features and the hematological problems (P3, P4 and P9) in our cohort have not been previously reported. Some of the new facial features described are likely due to the different ethnic background. Interestingly, the three patients with idiopathic thrombocytopenic purpura or anemia were all with 22q13.3 terminal deletions. It is not clear whether the hematological problem simply has not been studied in other studies or

specific to Chinese children. Alternatively, the hematological problem may be a secondary finding that is not related to the 22q13.3 deletions. The penetrance of ASD diagnosis in our *SHANK3* cohort (86 %) is slightly higher than that in other reports of non-Chinese children (84.4 %) with *SHANK3* defects (Soorya et al., 2013). This may be biased due to a relatively small sample size or due to the diagnostic methods for ASD used for the assesment in our study. In addition, the heterogeneity of genetic defects associated with *SHANK3* among different reports may also contribute to the difference.

Previous studies have also implicated a variety of gross structural abnormalities in brains of PMS patients. Some brain imaging reports include the clinical brain MRI in 8 patients with 22q13.3 deletions (Philippe et al., 2008b) and 24 patients with *SHANK3* loss of function mutations (Holder and Quach, 2016). These reports suggest the findings of atypical corpus callosum or hyperintensities of deep white matter. However, these findings were extracted from retrospective clinical chart review. The resolution of imaging was relatively low and quantitative analysis was not performed. A more recent DTI study in 12 *SHANK3*--deficient patients applying whole brain-based statistical analysis indicated decreased FA in superior longitudinal fasciculus, uncinate fasciculus and inferior fronto-occipital fasciculus (Jesse et al., 2020). The fiber tracking study in 10 patients with PMS reported FA decrease and MD increase in uncinate fasciculus (Bassell et al., 2020). However, the subjects with wide age ranges of 2–58 and 3–21 years respectively are studied in these studeis which may cause misspecification of segmented data, irregular registrations and the absence of appropriate stereotaxic volumes. Our study has designed to include participant with reasonable age-range (4.6 ± 2.3 years), generate study-and-age-specific brain templates and apply voxel-based full brain analysis, aiming to provided more robust and quantitative measurement of brain morphometry in SHANK3 group and controls (ASD controls and TD controls). In our study, VBM analysis revealed decreased grey matter volumes in dorsal striatum, amygdala, hippocampus, and parahippocampal gyrus in SHANK3 subjects compared to TD and ASD controls. Grey matter reduction was prominent in the dorsal striatum (caudate and putamen) which is the core component of corticostriatal circuit. These findings were consistent with previous studies in patients with PMS or *SHANK3* deficient patients (Srivastava et al., 2019). For the white matter, TBSS results demonstrated decreased FA in multiple tracts with projection, association and commissural fibers which surrounded the altered grey matter in SHANK3 group.

Convergent evidence elaborated that, for the corticostriatal projections, the intratelencephalic neurons project via the external capsule and corpus callosum within striatum and cortex, while the pyramidal tract neurons project via the internal capsule and cerebral peduncle (Shepherd, 2013). As a postsynaptic scaffolding protein of SHANK family (SHANK1–3), SHANK3 is expressed highest in the corticostriatal glutamatergic synapses (Monteiro and Feng, 2017; Peca et al., 2011; Shepherd, 2013). Previous neuroimaging studies in idiopathic ASD frequently report alterations of the corticostrial structures (Hanson et al., 2018; Moessner et al., 2007; Zhou et al., 2016). Dysfunction of the corticostriatal connectivity is considered as one of the most prominent circuits in psychiatric and neurodevelopmental disorders, especially in ASD (Shepherd, 2013). The correlation analysis between TBSS results and clinical phenotypes revealed positive correlations between FA values of overall

TBSS results and DQ of Griffith domains including social, language, fine motor and performance domain in SHANK3 group (Fig. 4 D–H and Supplementary Table 6).

In this study, total intracranial volume and FA value in children with *SHANK3* deficient were significantly reduced than those in idiopathic ASD or TD group. The molecular nature underlying these defects in SHANK3 deficiency ASD is not immediately clear. Future neuropathological study using postmortem brain tissues is warranted and may provide the insight. However, these findings were reminiscent of the similar reports from the studies of SHANK3 deficiency in rodent or non-human primate models (Pagani et al., 2019; Schoen et al., 2019; Tu et al., 2019; Wang et al., 2016; Zhou et al., 2019). The total brain volume as well as sub-regions of brain such as hippocampus and thalamus were reduced in *Shank3* complete knockout mice (Wang et al., 2016). The reduced FA values are also reported in multiple tracts including corticostriatal tract in *Shank3* mutant mice (Pagani et al., 2019; Wang et al., 2016). The cellular number or morphology are normal but the number of synapses are reduced multiple lines of *Shank3* mutant mice (Wang et al., 2011; Duffney et al., 2015; Jaramillo et al., 2016; Lee et al., 2015; Peca et al., 2011; Speed et al., 2015). In contrast, significant reductions of both synapse and neurons as well as neural connectivity are reported in SHANK3 monkey (Zhao et al., 2017; Tu et al., 2019; Zhou et al., 2019). These results are consistent with the reduced brain volume and FA value from brain imaging findings in SHANK3 deficient animals and suggest the similar molecular findings could be present in human *SHANK3* deficiency brain.

Our study also discovered significantly decreased grey matter volumes in amygdala and hippocampus in SHANK3 group. The amygdala was known to be crucial for normal social and emotional behaviors (Barak and Feng, 2016), while hippocampus plays a pivotal role in learning and memory (Benes, 2010; Cahill et al., 1996). The limbic system including amygdala and hippocampus have also been implicated in ASD and common comorbidity of anxiety and intellectual disability (Ecker et al., 2015; Varghese et al., 2017). The alteration of amygdala and hippocampus in SHANK3 group is consistent with high expression of *SHANK3* in these regions, the impaired synaptic function in hippocampal synapses in *Shank3* deficient mouse models (Peixoto et al., 2016; Wang et al., 2016), and the significant anxiety and intellectual disability in *SHANK3* related disorders in humans (Leblond et al., 2014; Soorya et al., 2013). Specially, the decreased amygdala and hippocampus volumes correlated with severity of restricted and repetitive behavior (RRB) in SHANK3 patients (Fig.4 A–B). There are caveats relate to this correlation analysis because of the small sample size and the variable size of chromosomal deletion and nature of genetic defects associated with *SHANK3*. Further investigation is warranted to replicate these findings in a large scale study. However, it is noted that the amygdala and hippocampus volumes were smaller in *Shank3* mutant mice which have significant repetitive behaviors (Wang et al., 2016). Together, the findings from both in human and mouse of model may support a causal correlation between these altered structures and ASD behaviors.

A few other limitations may also be considered. ASD due to *SHANK3* mutations is a relatively rare condition, thus enabling us to enroll only a small number of patients. To compensate, we tried to mitigate with a larger number of age and sex matched controls with a ratio of approximately 1:3 and with conservative statistical approaches. In addition, the

significant different DQ between SHANK3 group and idiopathic ASD controls may post a question whether the interpretation of the observed differences of brain structure between groups is confounded by the lower DQ in SHANK3 group. Although the inclusion of DQ as a covariant in the analysis of imaging data did support the low DQ in SHANK3 group is a strong modifier, the ideal design would be to include a group of idiopathic intellectual disability that is compatible SHANK3 group in future study. Furthermore, the current MRI scans were mainly structural. Thus, the results regarding underlying circuit dysfunctions need to be corroborated on brain functional connectivity such as resting state functional MRI studies. Despite these limitations, our results provide an initial informative assessment for the neuropathology of *SHANK3* deficiency in humans and provide a guidance to further understand the symptoms presented by these patients.

To conclude, we report for the first time that *SHANK3*-deficient ASD patients relate to the abnormal brain structures which could result in the disrupted striatum centered connectivity (Supplementary Fig. 1). These findings may support a path for further research to identify circuit dysfunctions and potential target areas for the novel therapeutic interventions. The study of monogenic ASD patients may offer insights into the diverse findings of previous neuroimaging studies of idiopathic ASD. Future studies of resting-state functional connectivity may allow for more in-depth understandings of the abnormal neural circuits and the underlying neuropathological mechanisms.

Supplementary Material

Refer to Web version on PubMed Central for supplementary material.

Acknowledgments

We are grateful to the children and parents who generously contributed their time to this research. We thank all members of the Division of Child Health Care of Children's Hospital of Fudan University in China for their help in aspects of participant recruitment, assessment and data collection and Department of Radiology for their technical support. We thank Xiang Yu (School of Life Sciences, Beijing University, China) for the guidance on the manuscript. We thank Zheng Wang (Institute of Neuroscience, Key Laboratory of Primate Neurobiology, CAS Center for Excellence in Brain Science and Intelligence Technology, Shanghai Institute for Biological Sciences, Chinese Academy of Sciences, China) for his suggestions of MRI data analysis. We also thank Dazhi Yin (School of Psychology and Cognitive Science, East China Normal University, China) and Qian Qin (Department of Pathology, Harvard Medical School, Boston, MA, USA) for advising on data analysis.

Grant support

This study was supported by grants from the National Key Research and Development Program of China (No. 2016YFC1306205), the National Natural Science Foundation of China (NSFC, No. 81371270) and the Machine Assisted System for Autism Spectrum Disorder Diagnosis and Treatment (No. 61733011) to Xiu Xu. This study was also supported by grants from the Shanghai Sailing Program (NO.19YF1403800) and Clinical Research of Shanghai Municipal Health Commission (NO. 20204Y0102) to Chunxue Liu and the National Natural Science Foundation of China (NSFC, No. 81701129) to Dongyun Li.

Data accessibility

All data used for this study are preserved at the Department of Child Health Care of Children's Hospital of Fudan University. Data are accessible on demand as far as allowed by guidelines of the ethics committee of the Children's Hospital of Fudan University. Requests should be addressed to the corresponding author Xiu Xu.

Abbreviations:

SHANK3	SH3 and multiple ankyrin repeat domains 3
ASD	autism spectrum disorder
TD	typically developing
ADOS-2	autism diagnostic observation schedule-the second edition
DTI	diffusion tensor imaging
VBM	voxel-based morphometry
TBSS	tract-based spatial statistics
FA	fractional anisotropy
MD	mean diffusivity
AAL	automated anatomical labeling
JHU	Johns Hopkins University
DQ	total development quotient
TIV	total intracranial volume
IQR	image quality rating
FD	framewise displacement

References

Aoki Y, Yoncheva YN, Chen B, Nath T, Sharp D, Lazar M, Velasco P, Milham MP, Di Martino A, 2017. Association of white matter structure with autism Spectrum disorder and Attention-Deficit/Hyperactivity disorder. JAMA Psychiat. 74, 1120–1128.

Ashburner J, 2007. A fast diffeomorphic image registration algorithm. Neuroimage 38, 95–113. [PubMed: 17761438]

Barak B, Feng G, 2016. Neurobiology of social behavior abnormalities in autism and Williams syndrome. Nat. Neurosci 19, 647–655. [PubMed: 29323671]

Bassell J, Srivastava S, Prohl AK, Scherrer B, Kapur K, Filip-Dhima R, Berry-Kravis E, Soorya L, Thurm A, Powell CM, Bernstein JA, Buxbaum JD, Kolevzon A, Warfield SK, Sahin M, 2020. Diffusion tensor imaging abnormalities in the uncinate fasciculus and inferior longitudinal fasciculus in Phelan-McDermid syndrome. Pediatr. Neurol 106, 24–31. [PubMed: 32107139]

Benatti A, Ferrari F, Giustardi A, Filippi A, Pinelli M, Bosi R, Modena N, Cavazzuti GB, 1986. Griffith test in the evaluation of psychomotor development in the 1st year of life. A longitudinal study. Pediatr. Med. Chir 8, 757–761. [PubMed: 3601706]

Benes FM, 2010. Amygdalocortical circuitry in schizophrenia: from circuits to molecules. Neuropsychopharmacol 35, 239–257.

Betancur C, Buxbaum JD, 2013. SHANK3 haploinsufficiency: a “common” but underdiagnosed highly penetrant monogenic cause of autism spectrum disorders. Mol. Autism 4, 17. [PubMed: 23758743]

Bonaglia MC, Giorda R, Beri S, De Agostini C, Novara F, Fichera M, Grillo L, Galesi O, Vetro A, Ciccone R, Bonati MT, Giglio S, Guerrini R, Osimani S, Marelli S, Zucca C, Grasso R, Borgatti

R, Mani E, Motta C, Molteni M, Romano C, Greco D, Reitano S, Baroncini A, Lapi E, Cecconi A, Arrigo G, Patricelli MG, Pantaleoni C, D'Arrigo S, Riva D, Sciacca F, Dalla BB, Zoccante L, Darra F, Termine C, Maserati E, Bigoni S, Priolo E, Bottani A, Gimelli S, Bena F, Brusco A, di Gregorio E, Bagnasco I, Giussani U, Nitsch L, Politi P, Martinez-Frias ML, Martinez-Fernandez ML, Martinez GN, Bremer A, Anderlid BM, Zuffardi O, 2011. Molecular mechanisms generating and stabilizing terminal 22q13 deletions in 44 subjects with Phelan/McDermid syndrome. PLoS Genet. 7, e1002173. [PubMed: 21779178]

Bostan AC, Dum RP, Strick PL, 2013. Cerebellar networks with the cerebral cortex and basal ganglia. Trends Cogn. Sci 17, 241–254. [PubMed: 23579055]

Cahill L, Haier RJ, Fallon J, Alkire MT, Tang C, Keator D, Wu J, McGaugh JL, 1996. Amygdala activity at encoding correlated with long-term, free recall of emotional information. Proc. Natl. Acad. Sci. U. S. A 93, 8016–8021. [PubMed: 8755595]

Chana G, Laskaris L, Pantelis C, Gillett P, Testa R, Zantomio D, Burrows EL, Hannan AJ, Everall IP, Skafidas E, 2015. Decreased expression of mGluR5 within the dorsolateral prefrontal cortex in autism and increased microglial number in mGluR5 knockout mice: pathophysiological and neurobehavioral implications. Brain Behav. Immun 49, 197–205. [PubMed: 26052099]

D'Albis MA, Guevara P, Guevara M, Laidi C, Boisgontier J, Sarrazin S, Duclap D, Delorme R, Bolognani F, Czech C, Bouquet C, Ly-Le MM, Holiga S, Amestoy A, Scheid I, Gaman A, Leboyer M, Poupon C, Mangin JF, Houenou J, 2018. Local structural connectivity is associated with social cognition in autism spectrum disorder. Brain 141, 3472–3481. [PubMed: 30423029]

De Rubeis S, Siper PM, Durkin A, Weissman J, Muratet F, Halpern D, Trelles M, Frank Y, Lozano R, Wang AT, Holder JJ, Betancur C, Buxbaum JD, Kolevzon A, 2018. Delineation of the genetic and clinical spectrum of Phelan-McDermid syndrome caused by SHANK3 point mutations. Mol. Autism 9, 31. [PubMed: 29719671]

Delahaye A, Toutain A, Aboura A, Dupont C, Tabet AC, Benzacken B, Elion J, Verloes A, Pipiras E, Drunat S, 2009. Chromosome 22q13.3 deletion syndrome with a de novo interstitial 22q13.3 cryptic deletion disrupting SHANK3. Eur. J. Med. Genet 52, 328–332.

Duffney LJ, Zhong P, Wei J, Matas E, Cheng J, Qin L, Ma K, Dietz DM, Kajiwara Y, Buxbaum JD, Yan Z, 2015. Autism-like deficits in Shank3-Deficient mice are rescued by targeting actin regulators. Cell Rep. 11, 1400–1413. [PubMed: 26027926]

Durand CM, Betancur C, Boeckers TM, Bockmann J, Chaste P, Fauchereau F, Nygren G, Rastam M, Gillberg IC, Anckarsater H, Sponheim E, Goubran-Botros H, Delorme R, Chabane N, Mouren-Simeoni MC, de Mas P, Bieth E, Roge B, Heron D, Burglen L, Gillberg C, Leboyer M, Bourgeron T, 2007. Mutations in the gene encoding the synaptic scaffolding protein SHANK3 are associated with autism spectrum disorders. Nat. Genet 39, 25–27. [PubMed: 17173049]

Ecker C, Bookheimer SY, Murphy DG, 2015. Neuroimaging in autism spectrum disorder: brain structure and function across the lifespan. Lancet Neurol. 14, 1121–1134. [PubMed: 25891007]

Gotham K, Risi S, Pickles A, Lord C, 2007. The autism diagnostic observation schedule: revised algorithms for improved diagnostic validity. J. Autism Dev. Disord 37, 613–627. [PubMed: 17180459]

Grzadzinski R, Huerta M, Lord C, 2013. DSM-5 and autism spectrum disorders (ASDs): an opportunity for identifying ASD subtypes. Mol. Autism 4, 12. [PubMed: 23675638]

Hanson KL, Lew CH, Hrvoj-Mihic B, Groeniger KM, Halgren E, Bellugi U, Semendeferi K, 2018. Increased glia density in the caudate nucleus in williams syndrome: implications for frontostriatal dysfunction in autism. Dev. Neurobiol 78, 531–545. [PubMed: 29090517]

Hernandez LM, Rudie JD, Green SA, Bookheimer S, Dapretto M, 2015. Neural signatures of autism spectrum disorders: insights into brain network dynamics. Neuropsychopharmacol 40, 171–189.

Holder JJ, Quach MM, 2016. The spectrum of epilepsy and electroencephalographic abnormalities due to SHANK3 loss-of-function mutations. Epilepsia 57, 1651–1659. [PubMed: 27554343]

Jaramillo TC, Speed HE, Xuan Z, Reimers JM, Liu S, Powell CM, 2016. Altered striatal synaptic function and abnormal behaviour in Shank3 Exon4–9 deletion mouse model of autism. Autism Res. 9, 350–375. [PubMed: 26559786]

Jesse S, Muller HP, Schoen M, Asoglu H, Bockmann J, Huppertz HJ, Rasche V, Ludolph AC, Boeckers TM, Kassubek J, 2020. Severe white matter damage in SHANK3 deficiency: a human and translational study. Ann. Clin. Transl. Neurol 7, 46–58. [PubMed: 31788990]

Jiang YH, Ehlers MD, 2013. Modeling autism by SHANK gene mutations in mice. Neuron 78, 8–27. [PubMed: 23583105]

Jordan L, Jackson NA, Carter-Snell B, Gaul M, Wikas S, 2019. Pustular tinea id reaction. Cutis 103, E3–E4.

Leblond CS, Nava C, Polge A, Gauthier J, Huguet G, Lumbroso S, Giuliano F, Stordeur C, Depienne C, Mouzat K, Pinto D, Howe J, Lemiere N, Durand CM, Guibert J, Ey E, Toro R, Peyre H, Mathieu A, Amsellem F, Rastam M, Gillberg IC, Rappold GA, Holt R, Monaco AP, Maestrini E, Galan P, Heron D, Jacquette A, Afenjar A, Rastetter A, Brice A, Devillard F, Assouline B, Laffargue F, Lespinasse J, Chiesa J, Rivier F, Bonneau D, Regnault B, Zelenika D, Delepine M, Lathrop M, Sanlaville D, Schluth-Bolard C, Edery P, Perrin L, Tabet AC, Schmeisser MJ, Boeckers TM, Coleman M, Sato D, Szatmari P, Scherer SW, Rouleau GA, Betancur C, Leboyer M, Gillberg C, Delorme R, Bourgeron T, 2014. Meta-analysis of SHANK mutations in autism spectrum disorders: a gradient of severity in cognitive impairments. PLoS Genet. 10, e1004580. [PubMed: 25188300]

Lee J, Chung C, Ha S, Lee D, Kim DY, Kim H, Kim E, 2015. Shank3-mutant mice lacking exon 9 show altered excitation/inhibition balance, enhanced rearing, and spatial memory deficit. Front. Cell. Neurosci 9, 94. [PubMed: 25852484]

Lek M, Karczewski KJ, Minikel EV, Samocha KE, Banks E, Fennell T, O'Donnell-Luria AH, Ware JS, Hill AJ, Cummings BB, Tukiainen T, Birnbaum DP, Kosmicki JA, Duncan LE, Estrada K, Zhao F, Zou J, Pierce-Hoffman E, Berghout J, Cooper DN, Deflaux N, DePristo M, Do R, Flannick J, Fromer M, Gauthier L, Goldstein J, Gupta N, Howrigan D, Kiezun A, Kurki MI, Moonshine AL, Natarajan P, Orozco L, Peloso GM, Poplin R, Rivas MA, Ruano-Rubio V, Rose SA, Ruderfer DM, Shakir K, Stenson PD, Stevens C, Thomas BP, Tiao G, Tusie-Luna MT, Weisburd B, Won HH, Yu D, Altshuler DM, Ardissino D, Boehnke M, Danesh J, Donnelly S, Elosua R, Florez JC, Gabriel SB, Getz G, Glatt SJ, Hultman CM, Kathiresan S, Laakso M, McCarroll S, McCarthy MI, McGovern D, McPherson R, Neale BM, Palotie A, Purcell SM, Saleheen D, Scharf JM, Sklar P, Sullivan PF, Tuomilehto J, Tsuang MT, Watkins HC, Wilson JG, Daly MJ, MacArthur DG, 2016. Analysis of protein-coding genetic variation in 60,706 humans. Nature 536, 285–291. [PubMed: 27535533]

Li D, Karnath HO, Xu X, 2017. Candidate biomarkers in children with autism Spectrum disorder: a review of MRI studies. Neurosci. Bull 33, 219–237. [PubMed: 28283808]

Liu Y, Liang M, Zhou Y, He Y, Hao Y, Song M, Yu C, Liu H, Liu Z, Jiang T, 2008. Disrupted small-world networks in schizophrenia. BRAIN 131, 945–961. [PubMed: 18299296]

Liu C, Li C, Hu C, Wang Y, Lin J, Jiang Y, Li Q, Xu X, 2018. CRISPR/Cas9-induced shank3b mutant zebrafish display autism-like behaviors. Mol. Autism 9.

Lord C, Rutter M, Le Couteur A, 1994. Autism Diagnostic Interview-Revised: a revised version of a diagnostic interview for caregivers of individuals with possible pervasive developmental disorders. J. Autism Dev. Disord 24, 659–685. [PubMed: 7814313]

Mahmood A, Bibat G, Zhan AL, Izbudak I, Farage L, Horska A, Mori S, Naidu S, 2010. White matter impairment in Rett syndrome: diffusion tensor imaging study with clinical correlations. AJNR Am. J. Neuroradiol 31, 295–299. [PubMed: 19833797]

Maillard AM, Ruef A, Pizzagalli F, Migliavacca E, Hippolyte L, Adaszewski S, Dukart J, Ferrari C, Conus P, Mannik K, Zazhytska M, Siffredi V, Maeder P, Kutalik Z, Kherif F, Hadjikhani N, Beckmann JS, Reymond A, Draganski B, Jacquemont S, 2015. The 16p11.2 locus modulates brain structures common to autism, schizophrenia and obesity. Mol. Psychiatry 20, 140–147. [PubMed: 25421402]

Moessner R, Marshall CR, Sutcliffe JS, Skaug J, Pinto D, Vincent J, Zwaigenbaum L, Fernandez B, Roberts W, Szatmari P, Scherer SW, 2007. Contribution of SHANK3 mutations to autism spectrum disorder. Am. J. Hum. Genet 81, 1289–1297. [PubMed: 17999366]

Monteiro P, Feng G, 2017. SHANK proteins: roles at the synapse and in autism spectrum disorder. Nat. Rev. Neurosci 18, 147–157. [PubMed: 28179641]

Muhle RA, Reed HE, Stratigos KA, Veenstra-VanderWeele J, 2018. The emerging clinical neuroscience of autism spectrum disorder: a review. Jama psychiat. 75, 514–523.

Muller RA, Fishman I, 2018. Brain connectivity and neuroimaging of social networks in autism. Trends Cogn. Sci 22, 1103–1116. [PubMed: 30391214]

Oberman LM, Boccuto L, Cascio L, Sarasua S, Kaufmann WE, 2015a. Autism spectrum disorder in Phelan-McDermid syndrome: initial characterization and genotype-phenotype correlations. Orphanet J. Rare Dis 10, 105. [PubMed: 26306707]

Oberman LM, Boccuto L, Cascio L, Sarasua S, Kaufmann WE, 2015b. Autism spectrum disorder in Phelan-McDermid syndrome: initial characterization and genotype-phenotype correlations. Orphanet J. Rare Dis 10, 105. [PubMed: 26306707]

Pagani M, Bertero A, Liska A, Galbusera A, Sabbioni M, Barsotti N, Colenbier N, Marinazzo D, Scattoni ML, Pasqualetti M, Gozzi A, 2019. Deletion of autism risk gene Shank3 disrupts prefrontal connectivity. J. Neurosci 39, 5299–5310. [PubMed: 31061091]

Peca J, Feliciano C, Ting JT, Wang W, Wells MF, Venkatraman TN, Lascola CD, Fu Z, Feng G, 2011. Shank3 mutant mice display autistic-like behaviours and striatal dysfunction. Nature 472, 437–442. [PubMed: 21423165]

Peixoto RT, Wang W, Croney DM, Kozorovitskiy Y, Sabatini BL, 2016. Early hyperactivity and precocious maturation of corticostriatal circuits in Shank3B(−/−) mice. Nat. Neurosci 19, 716–724. [PubMed: 26928064]

Phelan MC, 2008. Deletion 22q13.3 syndrome. Orphanet J. Rare Dis 3, 14. [PubMed: 18505557]

Phelan K, McDermid HE, 2012a. The 22q13.3 deletion syndrome (Phelan-McDermid syndrome). Mol. Syndromol 2, 186–201. [PubMed: 22670140]

Phelan K, McDermid HE, 2012b. The 22q13.3 deletion syndrome (Phelan-McDermid syndrome). Mol. Syndromol 2, 186–201. [PubMed: 22670140]

Philippe A, Boddaert N, Vaivre-Douret L, Robel L, Danon-Boileau L, Malan V, de Blois MC, Heron D, Colleaux L, Golse B, Zilbovicius M, Munnich A, 2008a. Neurobehavioral profile and brain imaging study of the 22q13.3 deletion syndrome in childhood. Pediatrics 122, e376–e382. [PubMed: 18625665]

Philippe A, Boddaert N, Vaivre-Douret L, Robel L, Danon-Boileau L, Malan V, de Blois MC, Heron D, Colleaux L, Golse B, Zilbovicius M, Munnich A, 2008b. Neurobehavioral profile and brain imaging study of the 22q13.3 deletion syndrome in childhood. Pediatrics 122, e376–e382. [PubMed: 18625665]

Sarasua SM, Dwivedi A, Boccuto L, Rollins JD, Chen CF, Rogers RC, Phelan K, DuPont BR, Collins JS, 2011. Association between deletion size and important phenotypes expands the genomic region of interest in Phelan-McDermid syndrome (22q13 deletion syndrome). J. Med. Genet 48, 761–766. [PubMed: 21984749]

Sarasua SM, Boccuto L, Sharp JL, Dwivedi A, Chen C, Rollins JD, Rogers RC, Phelan K, DuPont BR, 2014a. Clinical and genomic evaluation of 201 patients with Phelan–McDermid syndrome. Hum. Genet 133, 847–859. [PubMed: 24481935]

Sarasua SM, Dwivedi A, Boccuto L, Chen CF, Sharp JL, Rollins JD, Collins JS, Rogers RC, Phelan K, DuPont BR, 2014b. 22q13.2q13.32 genomic regions associated with severity of speech delay, developmental delay, and physical features in Phelan-McDermid syndrome. Genet. Med 16, 318–328. [PubMed: 24136618]

Schoen M, Asoglu H, Bauer HF, Muller HP, Abaei A, Sauer AK, Zhang R, Song TJ, Bockmann J, Kassubek J, Rasche V, Grabrucker AM, Boeckers TM, 2019. Shank3 transgenic and prenatal zinc-deficient autism mouse models show convergent and individual alterations of brain structures in MRI. Front. Neural Circuits 13, 6. [PubMed: 30853900]

Sheng M, Hoogenraad CC, 2007. The postsynaptic architecture of excitatory synapses: a more quantitative view. Annu. Rev. Biochem 76, 823–847. [PubMed: 17243894]

Shepherd GM, 2013. Corticostriatal connectivity and its role in disease. Nat. Rev. Neurosci 14, 278–291. [PubMed: 23511908]

Smith SM, Jenkinson M, Woolrich MW, Beckmann CF, Behrens TE, Johansen-Berg H, Bannister PR, De Luca M, Drobnjak I, Flitney DE, Niazy RK, Saunders J, Vickers J, Zhang Y, De Stefano N,

Brady JM, Matthews PM, 2004. Advances in functional and structural MR image analysis and implementation as FSL. Neuroimage 23 (Suppl 1), S208–S219. [PubMed: 15501092]

Smith SM, Johansen-Berg H, Jenkinson M, Rueckert D, Nichols TE, Miller KL, Robson MD, Jones DK, Klein JC, Bartsch AJ, Behrens TE, 2007. Acquisition and voxelwise analysis of multi-subject diffusion data with tract-based spatial statistics. Nat. Protoc 2, 499–503. [PubMed: 17406613]

Soorya L, Kolevzon A, Zweifach J, Lim T, Dobry Y, Schwartz L, Frank Y, Wang AT, Cai G, Parkhomenko E, Halpern D, Grodberg D, Angarita B, Willner JP, Yang A, Canitano R, Chaplin W, Betancur C, Buxbaum JD, 2013. Prospective investigation of autism and genotype-phenotype correlations in 22q13 deletion syndrome and SHANK3 deficiency. Mol. Autism 4, 18. [PubMed: 23758760]

Speed HE, Kouser M, Xuan Z, Reimers JM, Ochoa CF, Gupta N, Liu S, Powell CM, 2015. Autism-associated insertion mutation (InsG) of Shank3 exon 21 causes impaired synaptic transmission and behavioral deficits. J. Neurosci 35, 9648–9665. [PubMed: 26134648]

Srivastava S, Scherrer B, Prohl AK, Filip-Dhima R, Kapur K, Kolevzon A, Buxbaum JD, Berry-Kravis E, Soorya L, Thurm A, Powell CM, Bernstein JA, Warfield SK, Sahin M, 2019. Volumetric analysis of the basal ganglia and cerebellar structures in patients with Phelan-McDermid syndrome. Pediatr. Neurol 90, 37–43. [PubMed: 30396833]

Swanson MR, Wolff JJ, Shen MD, Styner M, Estes A, Gerig G, McKinstry RC, Botteron KN, Piven J, Hazlett HC, 2018. Development of white matter circuitry in infants with fragile X syndrome. JAMA Psychiat. 75, 505–513.

Tabet AC, Rolland T, Ducloy M, Levy J, Buratti J, Mathieu A, Haye D, Perrin L, Dupont C, Passemard S, Capri Y, Verloes A, Drunat S, Keren B, Mignot C, Marey I, Jacquette A, Whalen S, Pipiras E, Benzacken B, Chantot-Bastaraud S, Afenjar A, Heron D, Le Caignec C, Beneteau C, Pichon O, Isidor B, David A, El KL, Kemeny S, Gouas L, Vago P, Mosca-Boidron AL, Faivre L, Missirian C, Philip N, Sanlaville D, Edery P, Satre V, Coutton C, Devillard F, Dieterich K, Vuillaume ML, Rooryck C, Lacombe D, Pinson L, Gatinois V, Puechberty J, Chiesa J, Lespinasse J, Dubourg C, Quelin C, Fradin M, Journel H, Toutain A, Martin D, Benmansour A, Leblond CS, Toro R, Amsellem F, Delorme R, Bourgeron T, 2017. A framework to identify contributing genes in patients with Phelan-McDermid syndrome. NPJ Genom. Med 2, 32. [PubMed: 29263841]

Tu Z, Zhao H, Li B, Yan S, Wang L, Tang Y, Li Z, Bai D, Li C, Lin Y, Li Y, Liu J, Xu H, Guo X, Jiang YH, Zhang YQ, Li XJ, 2019. CRISPR/Cas9-mediated disruption of SHANK3 in monkey leads to drug-treatable autism-like symptoms. Hum. Mol. Genet 28, 561–571. [PubMed: 30329048]

Tzourio-Mazoyer N, Landeau B, Papathanassiou D, Crivello F, Etard O, Delcroix N, Mazoyer B, Joliot M, 2002. Automated anatomical labeling of activations in SPM using a macroscopic anatomical parcellation of the MNI MRI single-subject brain. Neuroimage 15, 273–289. [PubMed: 11771995]

Utter AA, Basso MA, 2008. The basal ganglia: an overview of circuits and function. Neurosci. Biobehav. Rev 32, 333–342. [PubMed: 17202023]

Varghese M, Keshav N, Jacot-Descombes S, Warda T, Wicinski B, Dickstein DL, Harony-Nicolas H, De Rubeis S, Drapeau E, Buxbaum JD, Hof PR, 2017. Autism spectrum disorder: neuropathology and animal models. Acta Neuropathol. 134, 537–566. [PubMed: 28584888]

Wakana S, Jiang H, Nagae-Poetscher LM, van Zijl PC, Mori S, 2004. Fiber tract-based atlas of human white matter anatomy. Radiology 230, 77–87. [PubMed: 14645885]

Wang X, McCoy PA, Rodriguiz RM, Pan Y, Je HS, Roberts AC, Kim CJ, Berrios J, Colvin JS, Bousquet-Moore D, Lorenzo I, Wu G, Weinberg RJ, Ehlers MD, Philpot BD, Beaudet AL, Wetsel WC, Jiang YH, 2011. Synaptic dysfunction and abnormal behaviors in mice lacking major isoforms of Shank3. Hum. Mol. Genet 20, 3093–3108. [PubMed: 21558424]

Wang X, Bey AL, Katz BM, Badea A, Kim N, David LK, Duffney LJ, Kumar S, Mague SD, Hulbert SW, Dutta N, Hayrapetyan V, Yu C, Gaidis E, Zhao S, Ding JD, Xu Q, Chung L, Rodriguiz RM, Wang F, Weinberg RJ, Wetsel WC, Dzirasa K, Yin H, Jiang YH, 2016. Altered mGluR5-Homer scaffolds and corticostriatal connectivity in a Shank3 complete knockout model of autism. Nat. Commun 7, 11459. [PubMed: 27161151]

Wilke M, Holland SK, Altaye M, Gaser C, 2008. Template-O-Matic: a toolbox for creating customized pediatric templates. Neuroimage 41, 903–913. [PubMed: 18424084]

Willsey AJ, State MW, 2015. Autism spectrum disorders: from genes to neurobiology. Curr. Opin. Neurobiol 30, 92–99. [PubMed: 25464374]

Wilson HL, Crolla JA, Walker D, Artifoni L, Dallapiccola B, Takano T, Vasudevan P, Huang S, Maloney V, Yobb T, Quarrell O, McDermid HE, 2008. Interstitial 22q13 deletions: genes other than SHANK3 have major effects on cognitive and language development. Eur. J. Hum. Genet 16, 1301–1310. [PubMed: 18523453]

Wolff JJ, Swanson MR, Elison JT, Gerig G, Pruett JJ, Styner MA, Vachet C, Botteron KN, Dager SR, Estes AM, Hazlett HC, Schultz RT, Shen MD, Zwaigenbaum L, Piven J, 2017. Neural circuitry at age 6 months associated with later repetitive behavior and sensory responsiveness in autism. Mol. Autism 8, 8. [PubMed: 28316772]

Xu N, Lv H, Yang T, Du X, Sun Y, Xiao B, Fan Y, Luo X, Zhan Y, Wang L, Li F, Yu Y, 2020. A 29 Mainland Chinese cohort of patients with Phelan-McDermid syndrome: genotype-phenotype correlations and the role of SHANK3 haploinsufficiency in the important phenotypes. Orphanet J. Rare Dis 15, 335. [PubMed: 33256793]

Zhao H, Tu Z, Xu H, Yan S, Yan H, Zheng Y, Yang W, Zheng J, Li Z, Tian R, Lu Y, Guo X, Jiang YH, Li XJ, Zhang YQ, 2017. Altered neurogenesis and disrupted expression of synaptic proteins in prefrontal cortex of SHANK3-deficient non-human primate. Cell Res. 27, 1293–1297. [PubMed: 28741620]

Zhou Y, Kaiser T, Monteiro P, Zhang X, Van der Goes MS, Wang D, Barak B, Zeng M, Li C, Lu C, Wells M, Amaya A, Nguyen S, Lewis M, Sanjana N, Zhou Y, Zhang M, Zhang F, Fu Z, Feng G, 2016. Mice with Shank3 mutations associated with ASD and schizophrenia display both shared and distinct defects. Neuron 89, 147–162. [PubMed: 26687841]

Zhou Y, Sharma J, Ke Q, Landman R, Yuan J, Chen H, Hayden DS, Fisher JR, Jiang M, Menegas W, Aida T, Yan T, Zou Y, Xu D, Parmar S, Hyman JB, Fanucci-Kiss A, Meisner O, Wang D, Huang Y, Li Y, Bai Y, Ji W, Lai X, Li W, Huang L, Lu Z, Wang L, Anteraper SA, Sur M, Zhou H, Xiang AP, Desimone R, Feng G, Yang S, 2019. Atypical behaviour and connectivity in SHANK3-mutant macaques. Nature 570, 326–331. [PubMed: 31189958]

Zwanenburg RJ, Ruiter SA, van den Heuvel ER, Flapper BC, Van Ravenswaaij-Arts CM, 2016. Developmental phenotype in Phelan-McDermid (22q13.3 deletion) syndrome: a systematic and prospective study in 34 children. J. Neurodev. Disord 8, 16. [PubMed: 27118998]

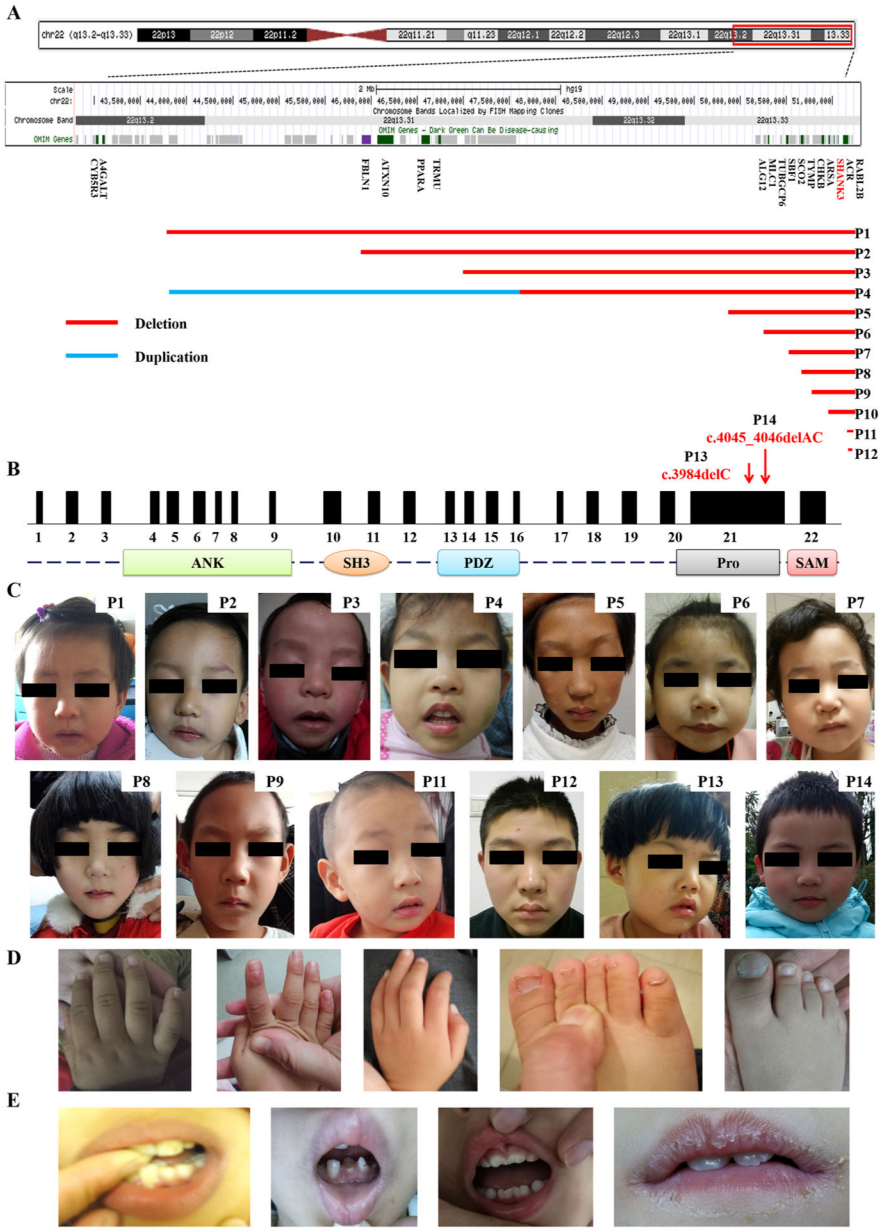

Fig. 1.

Genetic profile and the craniofacial features of 14 *SHANK3* deficient patients. **(A)** The size of deletions at 22q13.2–11q13.3 in 12 subjects. OMIM genes are indicated across the top in dark green and light grey. Dark green can be disease-causing. The location of *SHANK3* gene has been showed in red font. Patients 1 to 12 are listed on the right side. Red solid lines represent deletion and blue one represents duplication. The location of 22q13 cytogenetic bands and known genes are also presented in this figure produced using the UCSC genome browser. Genomic coordinates correspond to the hg19 genome assembly (Build 37) (color figure online). **(B)** Point mutations of *SHANK3* in P13 and P14 subjects. A diagram of the structure of *SHANK3* gene showing exon and intron structure and five conserved protein domains of ANK, ankyrin repeats; SH3, Src homology 3 domain; PSD, postsynaptic density

protein-95, Drosophila disk large tumor suppressor (DlgA) and Zonula occludens-1protein (Zo-1) domain proline-rich domain; SAM, sterile a-motif domain. **(C)** Common features of long and arched eyelashes, midface hypoplasia, wide nasal bridge, and anteverted nares. **(D)** Large fleshy hands and feet and dysplastic fingernails and toenails. **(E)** Dental hypoplasia or dysplasia.

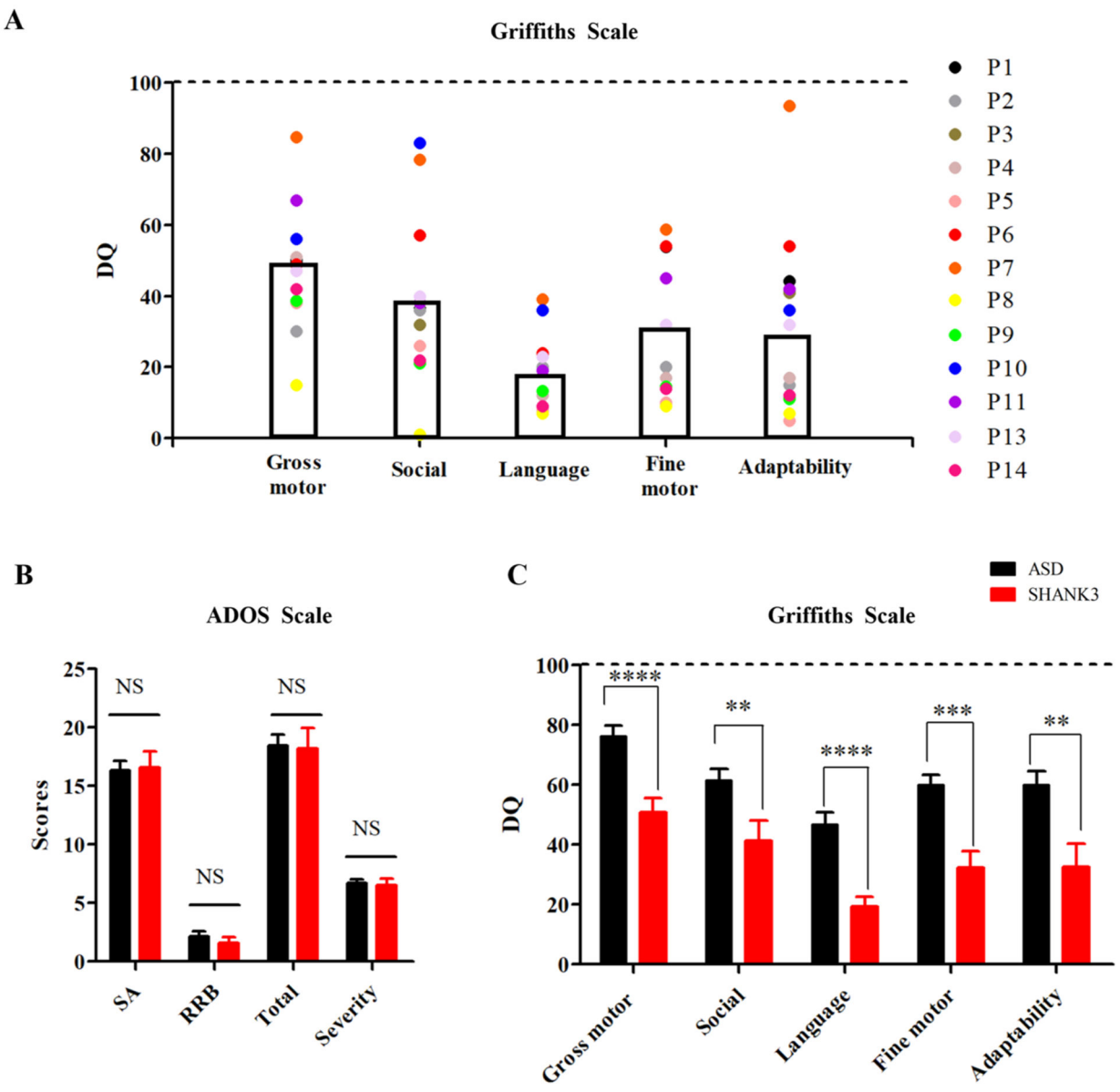

Fig. 2.

Clinical evaluations of *SHANK3* deficient patients and idiopathic ASD controls. **(A)** Developmental and cognitive assessment of *SHANK3* deficient patients using Griffiths scale. Dotted line represents the level of normal development children. Patients performed the best in the domain of gross motor and the poorest in the domain of listening and language (<1st percentile). 10 patients (71 %) presented absent speech with no ability to even consciously call mom and dad (0 words, P1–P9 and P14). 3 patients (21 %) could only speak 2–3 words, far behind the ability in the typical development children of their age (P10, P11 and P13). Only P12 (about 13 years old) can complete sentences, but with chaotic logic and less expressive, commentary or sharing tones. **(B–C)** Comparison between SHANK3 group and idiopathic ASD controls **(B)** AODS-2 domains (SHANK3 group: n = 12; ASD controls: n = 22) and **(C)** Griffiths domains (SHANK3 group: n = 11; ASD controls:

n = 20). Data represent mean ± standard deviation. Dotted line represents the level of normal development children. **P < 0.01; ***P < 0.001; ****p < 0.0001. ADOS-2, Autism Diagnostic Observation Schedule-The Second Edition; SA, social affect; RRB, restricted and repetitive behavior; NS, not significant.

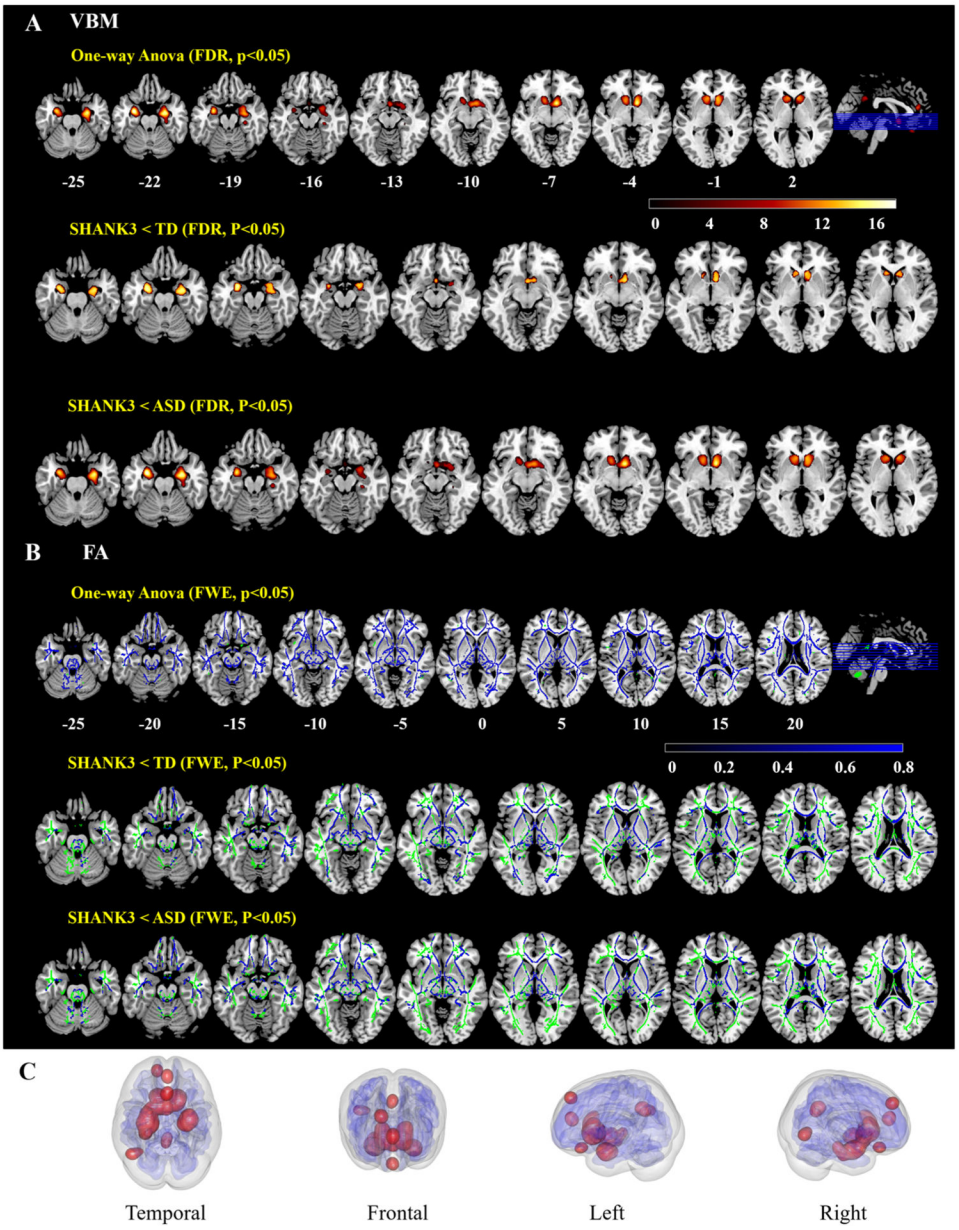

Fig. 3.

Neuroimaging findings of *SHANK3* deficient patients compared to idiopathic ASD and typically developing controls. These figures demonstrated the ANOVA and post-hoc statistical results of VBM analysis **(A)** and TBSS analysis **(B)** among three groups. **(A)** For VBM results, SHANK3 group showed significantly decreased grey matter volumes (red-yellow) compared with controls ($p < 0.05$, FDR corrected). **(B)** For TBSS results, SHANK3 group showed significantly decreased FA values (blue) compared with controls ($p < 0.05$, FWE corrected). Results are overlaid on MNI template (ch2better) and the mean FA skeleton (green). **(C)** The 3-dimensional visualization of VBM and TBSS results between SHANK3 group and ASD controls. VBM results were in red, FA results were in blue.

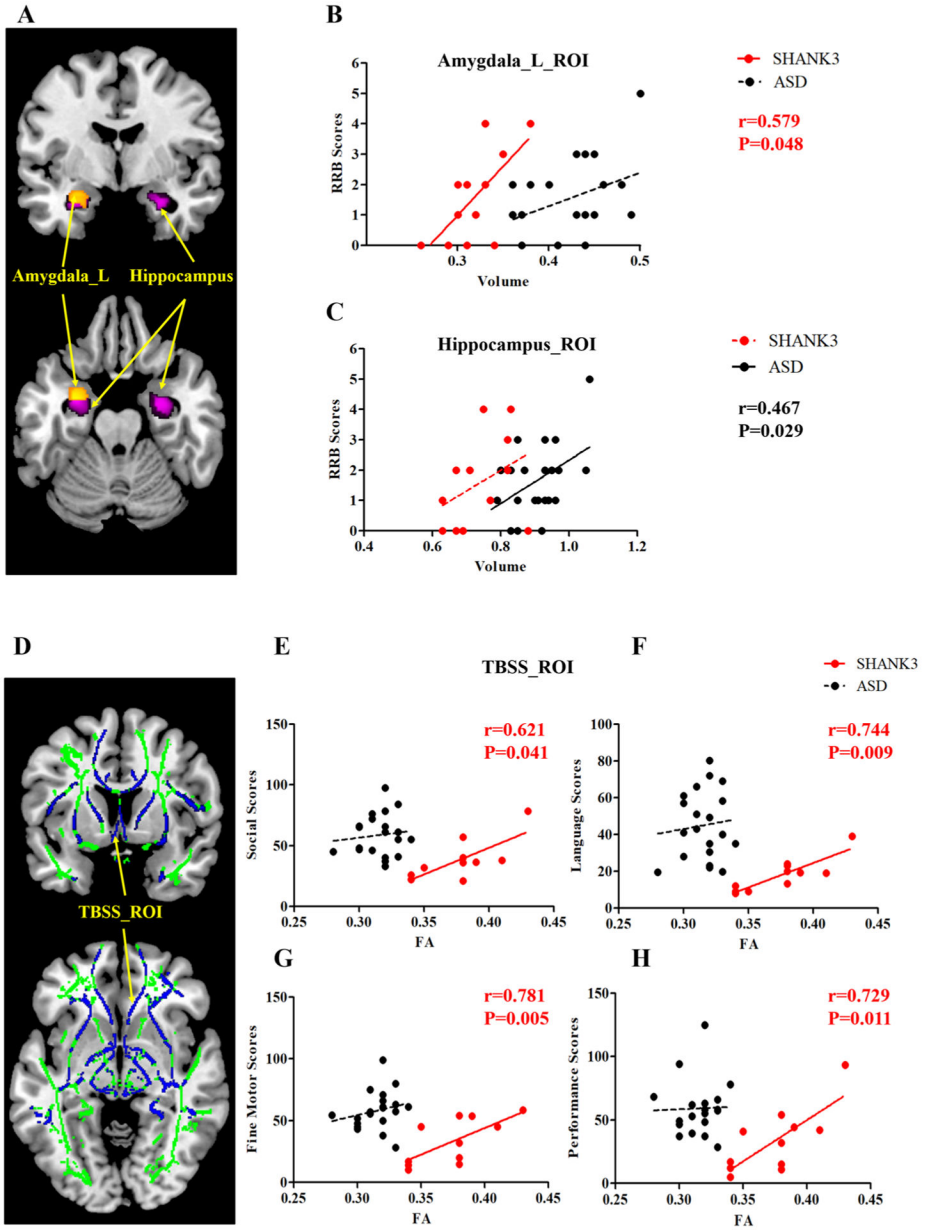

Fig. 4.

Correlations between brain structures and clinical data. (A–C) For grey matter: in the SHANK3 group, left amygdala volume (yellow) was positively associated with the RRB score (r = 0.579, $P = 0.048$) of ADOS; in the ASD group, hippocampus volume (violet) was positively associated with the RRB score (r=0.467, $P = 0.029$) of ADOS. Results are overlaid on MNI template (ch2better). (D–H) For the white matter, positive correlations found in the SHANK3 group but not in the ASD group were listed as follows: FA values of TBSS_all_ROI and DQ of social domain (r = 0.621, $P = 0.041$), DQ of language domain (r=0.744, $P = 0.009$), DQ of fine motor domain (r=0.781, $P = 0.005$) and DQ of performance

domain in Griffiths. Results (blue) are overlaid on MNI template (ch2better) and the mean FA skeleton (green).

Table 1

Summary of clinical characteristics of studying subjects.

	SHANK3 group	ASD group	TD group	P value
ADOS-2 Scale (individuals)	12	22	NA	
ASD severity	6.5 ± 1.67	6.68 ± 1.28	NA	0.570 [c]
SA	16.3 ± 3.86	15.59 ± 4.04	NA	0.720 [c]
RRB	1.58 ± 1.50	1.63 ± 1.17	NA	0.702 [c]
ADOS total score	17.92 ± 5.03	17.23 ± 4.46	NA	0.874 [c]
Griffith Scale (individuals)	11	20	NA	
Gross Motor	50.3 ± 15.08	73.39 ± 16.87	NA	**<0.0001** [c], ****
Social	37.16 ± 17.22	60.20 ± 17.25	NA	**0.002** [c], **
Language	17.79 ± 9.11	45.81 ± 19.35	NA	**<0.0001** [c], ****
Fine Motor	33.09 ± 18.65	57.71 ± 16.12	NA	**0.0004** [c], ***
Performance	33.34 ± 25.80	58.16 ± 22.47	NA	**0.006** [c], **
TIV	1244.93 ± 159.72	1375.61 ± 157.79	1359.71 ± 144.22	**0.044** [b], *
IQR	0.907 ± 0.006	0.906 ± 0.005	0.908 ± 0.006	0.653 [b]
FD	0.137 ± 0.025	0.140 ± 0.022	0.143 ± 0.021	0.709 [b]
FA	0.176 ± 0.015	0.196 ± 0.010	0.198 ± 0.012	**<0.0001** [b], ****
MD	1.064E-03 ± 0.050E-03	1.012E-03 ± 0.032E-03	1.006E-03 ± 0.043E-03	**0.0004** [b], ***
VBM				
Individuals	12	24	25	
Male : Female	6:6	20:4	19:6	0.095 [a]
Age (M±SD)	4.9 ± 3.2	4.0 ± 1.9	4.9 ± 2.4	0.322 [b]
TBSS				
Individuals	12	23	25	
Male : Female	6:6	20:3	15:10	**0.042** [a], *

	SHANK3 group	ASD group	TD group	P value
Age (M±SD)	4.9 ± 3.2	3.8 ± 1.8	4.8 ± 2.1	0.253[b]

ADOS-2, Autism Diagnostic Observation Schedule-The Second Edition; SA, social affect; RRB, restricted and repetitive behavior; IQR, image quality rating; FD, framewise displacement; TIV, total intracranial volume; VBM, voxel-based morphometry; TBSS, tract-based spatial statistics; FA, fractional anisotropy; MD, mean diffusivity; NA, not applicable.

[a] $\chi 2$ test.

[b] One-way ANOVA.

[c] Unpaired student's *t*-test (two-tailed).

* $p < 0.05$.

** $p < 0.01$.

*** $p < 0.001$.

**** $p < 0.0001$.

Table 2

Decreased grey matter volumes in comparisons between SHANK3 group and ASD controls for VBM analysis.

SHANK3 < ASD										
Cluster	1		2		3		4		5	
Number of voxels (AAL)	463		142		424		269		37	
Peak MNI coordinate	27,−6,−22.5		−30,−4.5,−22.5		9,10.5,−6		−9,21,−3		28.5,−84,4.5	
Peak MNI coordinate region	Hippocampus_R		Amygdala_L		Caudate_R		Caudate_L		Occipital_Mid_R	
Peak intensity	5.5009		5.3681		5.3198		4.7941		4.8546	
Other involved regions (name: voxels)	Hippocampus_R	234	Hippocampus_L	80	Caudate_R	314	Caudate_L	229	Occipital_Mid_R	37
	ParaHippocampal_R	181	Amygdala_L	62	Putamen_R	61	Putamen_L	40		
	Amygdala_R	48			Olfactory_R	45				
					Pallidum_R	4				

FDR corrected, $p < 0.05$.

Age, sex, total intracranial volume (TIV), total DQs and image quality rating (IQR) were included as covariates.

Table 3

Decreased fractional anisotropy values in comparisons between SHANK3 group and ASD controls for TBSS analysis.

SHANK3 < ASD								
			Peak					
Cluster Index	Voxels	P	MAX X (vox)	MAX Y (vox)	MAX Z (vox)	#	Atlas	Probability percentage
1	167,654	0.002	115	126	34	1	Middle_cerebellar_peduncle	4.39 %
						4	Body_of_corpus_callosum	3.85 %
						5	Splenium_of_corpus_callosum	3.57 %
						3	Genu_of_corpus_callosum	2.48 %
						26	Superior_corona_radiata_L	2.11 %
						25	Superior_corona_radiata_R	2.11 %
						24	Anterior_corona_radiata_L	1.92 %
						23	Anterior_corona_radiata_R	1.92 %
						41	Superior_longitudinal_fasciculus_R	1.85 %
						42	Superior_longitudinal_fasciculus_L	1.85 %
						33	External_capsule_R	1.57 %
						34	External_capsule_L	1.57 %
						30	Posterior_thalamic_radiation_L	1.12 %
						29	Posterior_thalamic_radiation_R	1.11 %
						19	Posterior_limb_of_internal_capsule_R	1.05 %
						20	Posterior_limb_of_internal_capsule_L	1.05 %
						27	Posterior_corona_radiata_R	1.05 %
						28	Posterior_corona_radiata_L	1.04 %
						17	Anterior_limb_of_internal_capsule_R	0.88 %
						18	Anterior_limb_of_internal_capsule_L	0.85 %
						36	Cingulum_(cingulate_gyrus)_L	0.77 %
						21	Retrolenticular_part_of_internal_capsule_R	0.71 %
						22	Retrolenticular_part_of_internal_capsule_L	0.69 %
						35	Cingulum_(cingulate_gyrus)_R	0.66 %
						15	Cerebral_peduncle_R	0.64 %
						16	Cerebral_peduncle_L	0.64 %

SHANK3 < ASD								
			Peak					
Cluster Index	Voxels	P	MAX X (vox)	MAX Y (vox)	MAX Z (vox)	#	Atlas	Probability percentage
						32	Sagittal_stratum_L	0.63 %
						31	Sagittal_stratum_R	0.63 %
						2	Pontine_crossing_tract_(a_part_of_MCP)	0.42 %
						8	Corticospinal_tract_L	0.38 %
						7	Corticospinal_tract_R	0.38 %
						37	Cingulum_(hippocampus)_R	0.35 %
						40	Fornix_(cres)_/_Stria_terminalis_L	0.32 %
						39	Fornix_(cres)_/_Stria_terminalis_R	0.32 %
						13	Superior_cerebellar_peduncle_R	0.28 %
						14	Superior_cerebellar_peduncle_L	0.28 %
						11	Inferior_cerebellar_peduncle_R	0.27 %
						12	Inferior_cerebellar_peduncle_L	0.27 %
						10	Medial_lemniscus_L	0.20 %
						6	Fornix_(column_and_body_of_fornix)	0.18 %
						48	Tapetum_L	0.17 %
						47	Tapetum_R	0.17 %
						43	Superior_fronto-occipital_fasciculus_R	0.14 %
						45	Uncinate_fasciculus_R	0.11 %
						46	Uncinate_fasciculus_L	0.11 %
2	20,956	0.004	137	132	78	25	Superior_corona_radiata_R	2.11 %
						23	Anterior_corona_radiata_R	1.92 %
						41	Superior_longitudinal_fasciculus_R	1.85 %

FWE corrected, $p < 0.05$.

Age, sex, total intracranial volume (TIV), total DQs and framewise displacement (FD) were included as covariates.